Applied Materials Today 37 (2024) 102147

Contents lists available at ScienceDirect

Applied Materials Today

journal homepage: www.elsevier.com/locate/apmt

Self-adhesive, ionic conductive, environmentally tolerant, and antibacterial phytic acid-reinforced zwitterionic hydrogels as flexible sensor applications

Zhenlin Zuo [a,b,c], Lei Song [a,b], Longxing Niu [a,b,*], Rong Wang [a,b,c,*]

[a] Zhejiang International Scientific and Technological Cooperative Base of Biomedical Materials and Technology, Institute of Biomedical Engineering, Ningbo Institute of Materials Technology and Engineering, Chinese Academy of Sciences, Ningbo 315201, PR China
[b] Ningbo Cixi Institute of Biomedical Engineering, Ningbo 315300, PR China
[c] University of Chinese Academy of Sciences, Beijing 101408, PR China

ARTICLE INFO

Keywords:
Ionic conductive hydrogels
Flexible sensors
Phytic acid
Zwitterionic hydrogels
Antibacterial

ABSTRACT

Ionic conductive hydrogels have attracted tremendous research interest for their intrinsic characteristics in the field of flexible sensors. However, the combination of multifunctionalities of high mechanical strength, satisfactory self-adhesiveness, ionic conductivity, anti-freezing, antibacterial properties, and biocompatibility remains a great challenge for the development of ionic conductive hydrogels. In this study, a novel ionic conductive hydrogel was developed by introducing highly conductive phytic acid (PA) to poly(sulfobetaine methacrylate) (polySBMA). PA molecules, as non-covalent crosslinkers and electrolytes in the polySBMA network, significantly improved the mechanical properties, self-adhesion, and electrical properties of the hydrogels. The optimal hydrogel displayed robust mechanical properties (tensile stress: 240.7 kPa), desirable adhesive strength (18.6 kPa to pig skin), and excellent ionic conductivity (2.44 S/m). Simultaneously, the presence of PA confers hydrogels with good antibacterial, anti-freezing properties and long-term environmental stability, and the hydrogels could remain soft even at -40 °C. Moreover, the hydrogel-based sensors showed high sensitivity (gauge factor up to 9.72), wide sensing range (≈400%), good stability, and accuracy for physical and physiological signals (tensile strain, pressure, fluid types and concentrations). This work has not only provided a simple strategy for fabricating tough and recoverable zwitterionic hydrogels, but also demonstrated the multifunctional properties of the zwitterionic hydrogels, which possess a great potential to fulfill flexible device applications.

1. Introduction

In recent years, flexible wearable devices that can conform to the deformation of integrated equipment due to their unique flexibility and ductility, are playing an important role in applications such as health monitoring, disease diagnosis and treatment, and human-computer interaction [1,2]. Flexible sensors, as the core component of wearable devices, need to integrate the fundamental functions of stretchability, flexibility, and good biocompatibility. Conductive hydrogels have been considered as ideal sensor materials due to their stretchable three-dimensional polymeric networks and customizability in structure and function [3,4]. Currently, numerous types of conductive hydrogels based on various conducting mechanisms, such as metal nanomaterials, carbon nanomaterials, conducting polymers, and ions have been developed [5]. Among them, ionic conductive hydrogels, which contain a large number of free ions from the polyelectrolyte or additional salts, are particularly attractive due to their ease of fabrication, low cost, wide sensing range, high transparency, and good biocompatibility. The conductivity of this type of hydrogel comes from the directional transportation of free ions similar to that of biosystems, and the excellent biocompatibility comes from their high water content and molecular similarity to natural soft tissues, which makes these ionic conductive hydrogels suitable for soft wearable or implantable sensors [6,7].

Among the various polymers available for the fabrication of ionic conductive hydrogels, zwitterionic polymers such as polysulfobetaine, polycarboxybetaine, and polyphosphobetaine have drawn particular interest in biological fields [8,9]. The ability to assist ion transportation along the highly depolarized polyzwitterionic skeleton endows

* Corresponding authors at: Zhejiang International Scientific and Technological Cooperative Base of Biomedical Materials and Technology, Institute of Biomedical Engineering, Ningbo Institute of Materials Technology and Engineering, Chinese Academy of Sciences, Ningbo 315201, PR China.
E-mail addresses: niulongxing@nimte.ac.cn (L. Niu), rong.wang@nimte.ac.cn (R. Wang).

https://doi.org/10.1016/j.apmt.2024.102147
Received 29 December 2023; Received in revised form 17 February 2024; Accepted 28 February 2024

polyzwitterionic hydrogels with high ionic conductivity [10]. Meanwhile, polyzwitterions with both positive and negative charges on polymer chains to make a high dipole moment entitle excellent adhesiveness of hydrogels to many surfaces [11]. Fu et al. [12] engineered a self-adhesive polyzwitterionic hydrogel using [2-(methacryloyloxy) ethyl]dimethyl(3-sulfopropyl) (SBMA) and acrylic acid (AA) monomers whose tensile strength, adhesive strength, and conductivity were 103.7 kPa, 10.5 kPa, and 7.4 S/m, respectively, showing the advantages of independent ionic conductivity, biocompatibility, transparency, and softness. However, most of the reported zwitterionic hydrogels are fragile with low fracture strain and under-perform in adhesion. In a previous study, the mechanical and adhesive properties of zwitterionic poly(sulfobetaine methacrylate) (polySBMA) hydrogels were improved by adding clay nanoflakes and tannic acid. Polyzwitterionic polymers cross-linked by dopamine-modified clay nanosheets exhibited a tensile strength of 90 kPa and a tissue adhesion strength of 19.4 kPa [11]. In contrast to the clay nanosheets, polySBMA hydrogel reinforced by tannic acid showed excellent mechanical property and strong adhesion, with the tensile stress and adhesive strength to skin tissue up to 93.7 kPa and 20.2 kPa, respectively. The presence of tannic acid also confers the hydrogels with antioxidant and antibacterial biological activities [13]. In addition, to optimize the conductivity and frost resistance of zwitterionic hydrogels, Yang et al. compounded 2-hydroxyethyl acrylate with SBMA in the presence of LiCl salt to form copolymer hydrogels, which exhibited a good ionic conductivity of 1.26 S/m at -40 °C [14]. According to the findings, polySBMA hydrogels can be functionalized in a variety of ways and potentially used as flexible sensors. Nevertheless, simultaneous integration of multiple functions such as mechanical suitability, adhesion properties, electrical conductivity, anti-freezing, antibacterial properties, and biocompatibility in the zwitterionic polySBMA hydrogels through a simple and convenient fabrication approach remains a challenge.

Phytic acid (PA) is a naturally occurring biocompatible substance extensively found in nuts, seeds, grains, and legumes. It can form supramolecular cross-linking structures with various molecules and metal ions through electrostatic interactions, hydrogen bonding, and coordination interactions, and improve the mechanical strength of hydrogels [15]. Additionally, as a six-fold dihydrogen phosphate ester of inositol, PA can dissociate twelve hydrogen ions (H^+) in three steps, allowing it to act as an ion donor when incorporated in hydrogels [16]. Currently, PA has been used as the electrolytes and cross-linking agents and directly compounded with polyacrylamide/chitosan [17], polyacrylamide/cellulose nanocrystals [18], polyvinyl alcohol (PVA) [19], polyvinyl alcohol/chitosan [20], and polyacrylic acid/carboxymethyl cellulose [21] to build ionic conductive hydrogels with tough mechanical properties, high conductivity, and good biocompatibility. Furthermore, PA can form strong hydrogen bonds with water molecules and suppress the formation of ice crystals at sub-zero temperatures. As a result, the addition of PA to the hydrogels may give them considerable flexibility and desirable characteristics at low temperatures [22]. Meanwhile, PA has antibacterial properties because its phosphate groups can form coordination interactions with Ca^{2+} and Mg^{2+} on the bacterial membrane, and the H^+ ions released from PA could enter the bacterial cells easily [23–25]. PA-incorporated hydrogels have shown excellent antibacterial activity against both Gram-positive and Gram-negative bacteria. For example, Liu et al. [26] created a skin-friendly conductive hydrogel with multiple hydrogen bonds by using biocompatible PVA, PA, and gelatin. It was shown that the introduction of PA endowed the hydrogel with conductivity and antibacterial properties. Based on these findings, it is expected that incorporating PA into hydrogels will give them good electrical conductivity, mechanical properties, anti-freezing, and antibacterial capabilities. Unfortunately, few attempts have been made to utilize this biomass-derived material for enhancing and functionalizing zwitterionic hydrogels.

In this work, a PA-reinforced zwitterionic polySBMA hydrogel was developed via a simple one-step free radical polymerization method. On the one hand, PA molecules were incorporated in the hydrogel as both non-covalent cross-linkers and electrolytes with the polySBMA network. On the other hand, the zwitterionic groups of SBMA promoted the ionization of H^+ from PA and provided channels for ion migration. The mechanical properties, transparency, self-adhesiveness, and electrical properties of PA-incorporated zwitterionic hydrogels were explored. Furthermore, the sensing performance, anti-freezing and antibacterial properties, and biocompatibility of the hydrogel, as well as the potential applications of the hydrogel as a flexible skin sensor, were investigated.

2. Materials and methods

2.1. Materials

[2-(Methacryloyloxy) ethyl] dimethyl-(3-sulfopropyl) ammonium hydroxide (SBMA, 97%), phytic acid (PA, 50 wt% in water), polyethylene glycol diacrylate (PEGDA, Mn=600, 98%), and 2-hydroxy-2-methylpropanone (97%) were purchased from Aladdin Chemistry (Shanghai, China). Artificial sweat (Catalogue No.: CF-001) was obtained from Chuangfeng Technology (Dongguan, China) and used as received. Deionized water with a resistivity of 18.2 MΩ•cm^{-1} was prepared using a Milli-Q Direct Ultrapure Water System from Millipore (Billerica, United States). All reagents were used directly as received without further purification. *Staphylococcus aureus* (*S. aureus*) 5622 was kindly provided by the First Affiliated Hospital of Ningbo University. *Escherichia coli* (*E. coli*) ATCC 25922 was obtained from American Type Culture Collection. NIH/3T3 fibroblast cells (Catalogue No.: SCSP-515) were bought from the National Collection of Authenticated Cell Cultures, Chinese Academy of Sciences.

2.2. Hydrogel preparation

Hydrogels were prepared using a straightforward one-pot free radical polymerization method. The precursor solution was prepared by mixing of 6.70 g SBMA monomer (24 mmol), 43.2 mg 2-hydroxy-2-methylpropanone (0.072 mmol), 11.8 mg PEGDA (0.072 mmol) and 50% PA solution (containing PA of 1.2, 2.4, 3.6, 4.8, and 6.0 mmol) with 6.0 mL deionized water. The precursor solution was poured into a reaction cell comprised of two glass plates (100 mm × 75 mm × 3 mm) sealed by a silicone rubber. Then the whole setup was irradiated under 365 nm ultraviolet light for 30 min for gelation. The obtained hydrogels were denoted as SP-x, where S stands for SBMA, P for PA, and x for the concentration of PA in the precursor solution. The SP-x hydrogels were sealed in plastic bags and stored at room temperature for further use.

2.3. Hydrogel mechanical property and transmittance

The tensile and compression properties of hydrogels were characterized using a Universal Testing Machine (CMT-1104, SUST, China). Hydrogel samples were cut into dumbbell shapes (gauge length of 12 mm, width of 2 mm, and thickness of 1 mm), and pulled at a rate of 100 mm/min until the break point. The toughness of each sample was calculated by integrating the area under the stress-strain curves. For the compression test, hydrogels were cut into cylinder shapes (10 mm in diameter and 1.8 mm in thickness) and compressed at a speed of 10% strain per min until 90% strain. Cyclic tensile tests (up to 200% of tensile strain) and cyclic compressive tests (up to 80% of compression strain) were conducted by cyclic loading and unloading of the samples in the Universal Testing Machine at the same experiment conditions as described above for up to 11 cycles. The dissipated energy was estimated by the integrated area of the hysteresis loop between each loading-unloading curve.

The transmission of hydrogel samples (thickness of 1 mm) was measured using a UV–Vis-NIR spectrophotometer (Cary 5000, Agilent, United States) with the scanning wavelength range of 380–800 nm, and

air transmittance was used as the baseline.

2.4. Self-adhesion tests

Lap shear tensile tests were performed on various substrates using a Universal Testing Machine (CMT-1104, SUST, China) to evaluate the adhesive strength of hydrogels. Briefly, a hydrogel specimen with a thickness of 1 mm was sandwiched between two substrates with an overlapping area of 2.5 cm × 2.0 cm, and pressed by a 100 g weight for 5 min. The specimens were pulled at a fixed speed of 50 mm/min until break. The adhesive strength was calculated from the measured maximum tensile force divided by the contact area of the sample (5.0 cm^2). The adhesive strength was calculated from the measured maximum tensile force divided by the contact area of the sample (5.0 cm^2). To test the cyclic adhesion properties of the hydrogel, the same adhesion experiment was repeated 5 times for each hydrogel sample.

A 90° peeling test was conducted to measure the adhesion between the hydrogels and solid substrates. The hydrogel samples were prepared into strips (width = 10 cm, thickness = 4 mm, length = 15 cm). A polyethylene terephthalate film was attached to one side of the hydrogel as a support to avoid deformation during the peeling process. The peeling speed of the test was 5 mm/s. The force-displacement curve of each sample was recorded.

2.5. Electrical property of hydrogels

All the hydrogel samples were cut into strips with the size of 20 mm × 5 mm × 1 mm. The electrical conductivity of the hydrogels was determined using a digital four-probe tester (ST2242, Jingge, China). The electrical measurement of the hydrogels was conducted by connecting an electrochemical workstation (PARSTAT 4000A, Princeton, USA) and loading in a universal testing machine at room temperature. The changes in the electrical resistance were recorded by the electrochemical workstation when the hydrogel was stretched or compressed repeatedly to a certain strain at a predetermined interval. The electrochemical impedance spectroscopy (EIS) measurement was carried out on an electrochemical workstation with a conventional three-electrode system, with the amplitude of 5 mV and the frequency ranging from 0.1 Hz to 10^5 Hz.

2.6. Sensing performance evaluation

To analyze the sensing performance, hydrogels (20 mm × 5 mm × 1 mm) were adhered onto a volunteer's joint (elbow, throat, finger, etc.), and connected by two electrodes to the electrochemical workstation. The experiments were conducted with the consent of the volunteer. The changes in the electrical resistance of the hydrogel during the joint motion, swallowing, and speaking of the volunteer were recorded.

The sensitivity of the hydrogels on physiological fluids was investigated by dropping the liquids (deionized water, NaCl solution, phosphate-buffered saline (PBS, 10 mM, pH 7.4), and artificial sweat) onto the hydrogel, which was connected to an electrochemical workstation, and the change in relative resistance of the hydrogel was recorded. The above experimental data were calculated as the relative resistance change rate ($\Delta R/R_0$) according to the following equation:

$$\frac{\Delta R}{R_0} = \frac{R - R_0}{R_0} \times 100\%$$

Where R_0 and R represent the resistance of the original and deformed hydrogels, respectively.

2.7. Anti-freezing test and long-term stability

The thermal properties of hydrogels were analyzed using a Differential Scanning Calorimetry (DSC, 2500, TA Instruments, United States), which was scanned from 40 °C to -89 °C at a cooling rate of 2 °C per min under a nitrogen atmosphere. The mechanical properties, self-adhesion performance, conductivity, and sensing performance of the hydrogel was tested as described above after it was stored at -20 °C for 24 h or in an environment with a temperature of 25 °C and relative humidity of 60% for 7 days.

2.8. Antibacterial assay

The hydrogels were cut into a disc with a diameter of 10 mm, washed twice with distilled water, and sterilized under ultraviolet irradiation. *E. coli* and *S. aureus* were cultured in lysogeny broth and tryptic soy broth overnight, respectively. The diluted bacterial suspension (5×10^5 CFU/mL) was spread on the culture agar plates. The hydrogel disks (10 mm in diameter) were placed on the agar plates, and they were incubated at 37 °C for 24 h. The zone of inhibition around each hydrogel sample was measured.

2.9. Cytotoxicity assay

Cytotoxicity assay was carried out using NIH/3T3 fibroblasts. Cells was seeded in 96-well plates at a density of 1×10^5 cells per well and cultured in Dulbecco's modified Eagle's medium (DMEM, Gibco, USA), supplemented with 10% fetal bovine serum (FBS, Gibco, USA) and 1% antibiotics (penicillin and streptomycin) at 37 °C using a humidified 5% CO_2 incubator for 24 h. The sterile hydrogel samples were immersed in deionized water at a ratio of 25 mg/mL at 37 °C for 24 h. The collected hydrogel extract solution was then diluted with DMEM in a volume ratio of 1: 4. Subsequently, the mixture of medium and extract solution was used for cell culture. Deionized water/DMEM mixture, complete fresh medium, and medium with 10 mg/mL zinc diethyldithiocarbamate were used as the controls. After cultured for 24 h, cell counting kit-8 (CCK-8, TransGen Biotech, China) assay was performed to evaluate the cell viability, which was represented as a percentage of the absorbance value of the experimental group compared to the negative control group (deionized water/DMEM mixture).

2.10. In vivo skin irritation test

Male Kunming mice (25–30 g) were used and the procedures for animal experiments were approved by the Institutional Animal Care and Use Committee of Ningbo Institute of Life and Health. All animals had free access to standard food and water. The skin irritation test was conducted according to ISO 10993–10. The hair on the back of the mouse was shaved. SP-0 and SP-6 hydrogels (8 mm in diameter and 1 mm in thickness) was placed on the animal's skin and fixed using a Tegaderm dressing for 1 h. The appearance of the treated site was photographed after 1, 24, 48, and 72 h. All mice were euthanized peacefully after experiments. Tissue slices of 5 μm in thickness from the treated sites were obtained by paraffin section. Histological evaluation was conducted by hematoxylin and eosin (H&E, Solarbio G1120, China) staining, followed by microscope observation (DFC450 C, Leica, Germany).

3. Results and discussion

3.1. Hydrogel fabrication and mechanical property

SBMA monomers and PA were selected to prepare ionic conductive hydrogel by the one-pot free radical polymerization method. Upon UV irradiation, the initiator ammonium persulfate produced free radicals, which triggered the ultra-fast polymerization of zwitterionic SBMA monomers. A three-dimensional zwitterionic polySBMA network was formed through covalently cross-linked by PEGDA, and electrostatic interactions between the SBMA units (Fig. 1). In addition, PA could be ionized in water [19], and the charged phosphate groups in PA could

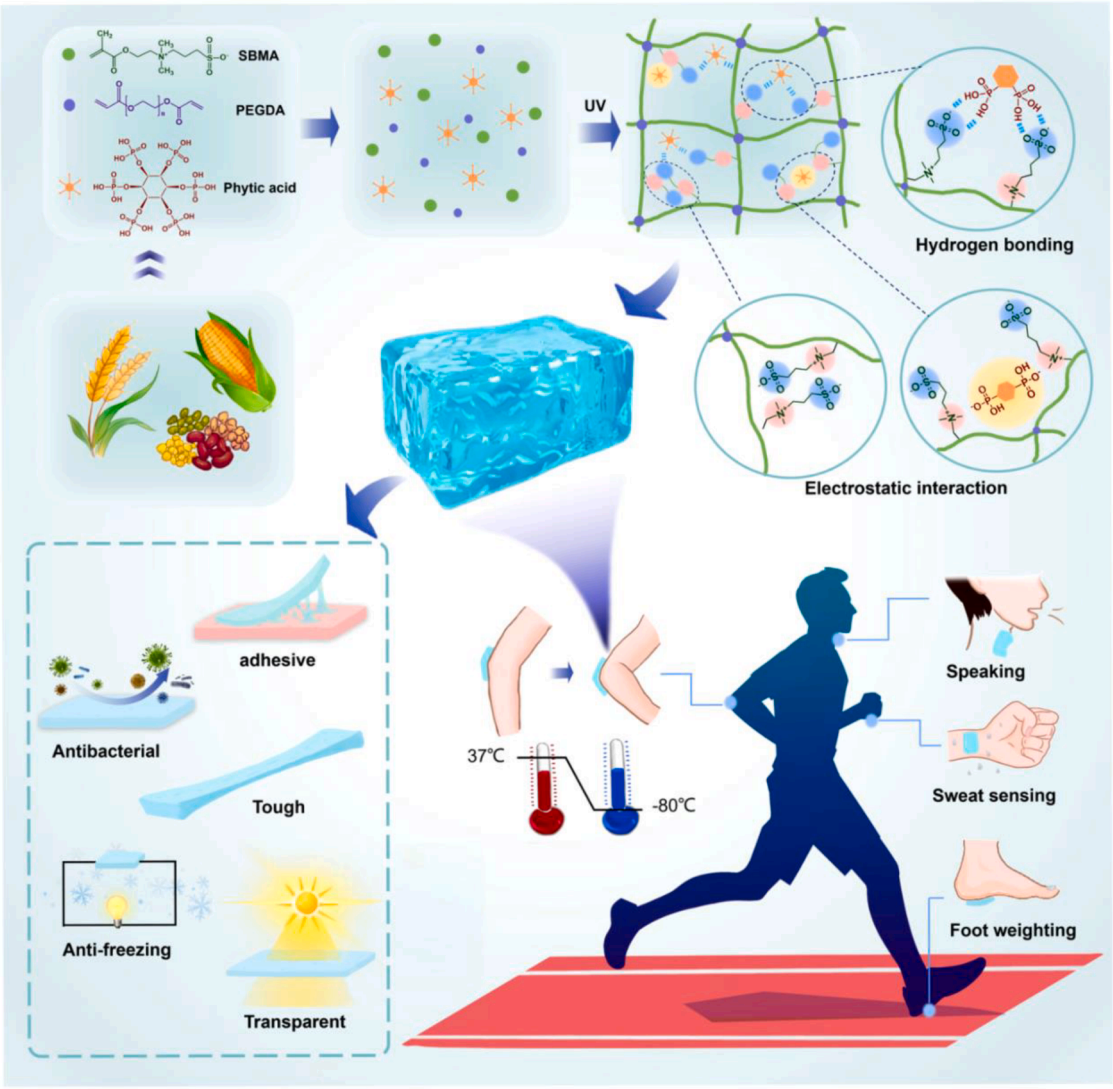

Fig. 1. Schematic illustration of the preparation process and potential applications of SP-x hydrogels.

form non-covalent interactions including electrostatic interactions and hydrogen bonding with the SBMA units in the network, thereby further cross-linking the hydrogel.

Excellent mechanical properties (tension and compression) are highly necessary for flexible hydrogel devices to adapt to arbitrary limb movements and avoid mechanical damage in actual applications. The SP-x hydrogel (SP-6 as demonstration) exhibited outstanding extensibility (Fig. 2a i-ii) and self-recovery capability after compression (Fig. 2a iii-v) in Fig. 2a. The tensile fracture stress of pure polySBMA hydrogel was 76.3 kPa, and it increased after addition of PA (Fig. 2b). As the PA content increased to 1.0 mol/L, the tensile fracture stress of SP-x hydrogel increased to 333.0 kPa (Fig. 2b), showing that the addition of PA could significantly improve the tensile properties of hydrogel. It was noted that the elastic modulus value of SP-x hydrogel was determined to be 31.3 kPa to 82.6 kPa (Fig. S1), which was in the range of the elastic modulus of human skin (1–100 kPa) [27], showing its potential to be used in skin sensor applications. The toughness of the hydrogels greatly increased with an increasing PA content from 129.8 kJ/m^3 (SP-0) to 342.6 kJ/m^3 (SP-6) (Fig. S2a), indicating their ability to withstand high stresses. For compression tests, with the PA content in the precursor increased from 0 to 1.0 mol/L, the compressive strength increased from 1.3 MPa to 4.2 MPa at 90% of compressive strain (Fig. 2c), which showed the addition of PA also significantly improve the compressive strength of hydrogel. The increase in mechanical strength of the SP-x hydrogel could be attributed to the formation of substantial non-covalent cross-linking (i.e., electrostatic interactions and hydrogen bonding) between the zwitterionic groups and PA molecules, which resulted in more tightly cross-linked polymer networks. In addition, the non-covalent interactions between PA and SBMA units also endow remarkable recovery and fatigue resistance to the hydrogels.

The mechanical endurability and structural stability of SP-x hydrogel were further investigated by cyclic loading-unloading tensile test and compression test on SP-6 hydrogel. The tensile stress-strain curves of SP-6 hydrogel almost coincide during the process of continuously increasing tensile strain from 100% to 300% (Fig. 2d), showing an amazing self-recovery ability. The hysteresis loop of SP-6 hydrogel under different strains was relatively small, which proved the high elasticity of hydrogel. In the cyclic tensile test, there was a slight decrease in the hysteresis and tensile strength after the first cycle of SP-6 hydrogel (Fig. 2e), the dissipated energy at the first stretching cycle was 8.2 J/m^3 (Fig. S2b), which may be caused by the breaking of the physical cross-linking network and drift of the polymer chains [21]. In the second and subsequent cycles, the hysteresis and tensile strength remained almost the same, with the dissipated energy between 4.1–4.7 J/m^3, indicating that the hydrogel recovered effectively. Over eleven continuous compression cycles, the stress-strain curve of SP-6 hydrogel almost

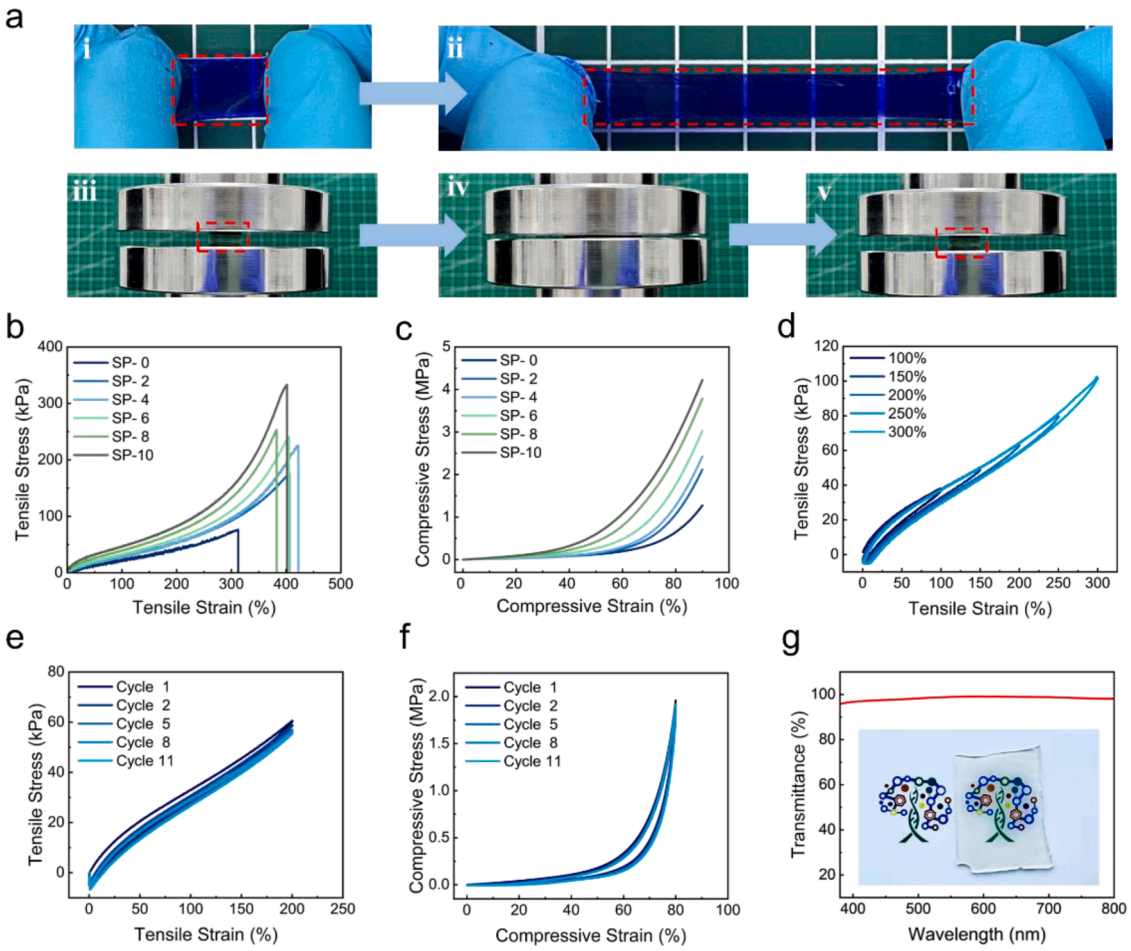

Fig. 2. (a) Photographs of SP-6 hydrogel (stained with methylene blue for better visualization) showing large stretchability and self-recovery ability. Representative (b) tensile and (c) compressive stress-strain curves of SP-x hydrogels. (d) Cyclic tensile loading-unloading curves of SP-6 hydrogel with gradual increase in strain (100, 150, 200, 250, and 300%). Successive (e) tensile and (f) compression loading-unloading curves of SP-6 hydrogel over 11 cycles. (g) Transmittance of SP-6 hydrogel with a thickness of 1 mm in the visible wavelength range of 380–800 nm. Inset showed an image of a transparent SP-6 hydrogel.

overlapped (Fig. 2f), and there is no significant difference in the dissipated energy in the eleven continuous compression cycles (Fig. S2c), indicating that the hydrogel had sufficient strength and toughness. All the above results demonstrate the remarkable recovery and fatigue resistance of the SP-6 hydrogel. The SP-x hydrogel also exhibited high transparency, with the transmittance of the SP-6 hydrogel being >95% at a wavelength range of 380–800 nm (Fig. 2g), which was conducive to targeting a specific area during the real-time monitoring of motions and signals.

3.2. Self-adhesiveness of SP-x hydrogel

Self-adhesiveness is another important property for flexible wearable sensors to be stable on the surface of the skin and other materials. As demonstrated in Fig. 3a, SP-6 hydrogel can adhere to the surfaces of various organic and inorganic materials, including plastic, copper, rubber, steel, polytetrafluoroethylene (PTFE) and glass. It also demonstrated robust and conformal adhesion on skin tissue even when subjected to bending and twisting. This excellent adhesion of SP-x hydrogel can be attributed to the synergistic effect of multiple non-covalent interactions between the SBMA groups and PA molecules of hydrogel and the functional groups on the various substrate surface (Fig. 3b). On the one hand, SBMA units contain cationic quaternary ammonium groups, anionic sulfonate groups and high dipole moments, all of which can interact with other charged or polar groups (e.g., Cu^{2+} of copper, $-NH_2^+$ and $-COO^-$ groups of skin, and C≡N groups of rubber) via ion-dipole and dipole-dipole interactions [28]. On the other hand, the increase in the content of phosphate groups from PA further enhanced the interactions with the substrate surface via hydrogen bonding and electrostatic interactions (e.g., –OH groups of glass and C-F groups of PTFE).

The adhesive strength of SP-x hydrogel on pig skin was quantified using a shear lap test (Fig. 3c). The adhesive strength of SP-0 on skin tissue was 8.9 kPa. When PA was added, the adhesive strength of the hydrogel increased from 10.6 kPa of SP-2 to a maximum of 18.6 kPa of SP-6, which is greater than that of clinically used fibrin glue (~12 kPa) [29]. This demonstrated that PA could help improve the adhesive strength of the hydrogels. The enhancement is mainly due to the formation of hydrogen bonding (–OH and PO_4^{3-} groups on PA with $–NH_2$ and –COOH groups on skin) and electrostatic interactions (PO_4^{3-} groups on PA with $–NH_2^+$ groups on skin) between the hydrogel and porcine skin (Fig. 3b). However, as the PA content continued to increase, the adhesive strength of SP-x hydrogel decreased. This may be due to the fact that the high PA content resulted in a dense cross-linking network and low flexibility of the hydrogel, making it difficult to adhere firmly to the skin surface. In addition, excessive cross-linking could reduce the free functional groups on the hydrogel surface, thus inhibiting the formation of non-covalent interactions at the hydrogel-skin interface. The above results indicated that SP-6 is a representative hydrogel with excellent self-adhesion properties and appropriate mechanical properties for sensor applications.

The force-displacement curves and quantitative values of adhesive strength of SP-6 hydrogel on pig skin, PTFE, rubber, glass, and copper

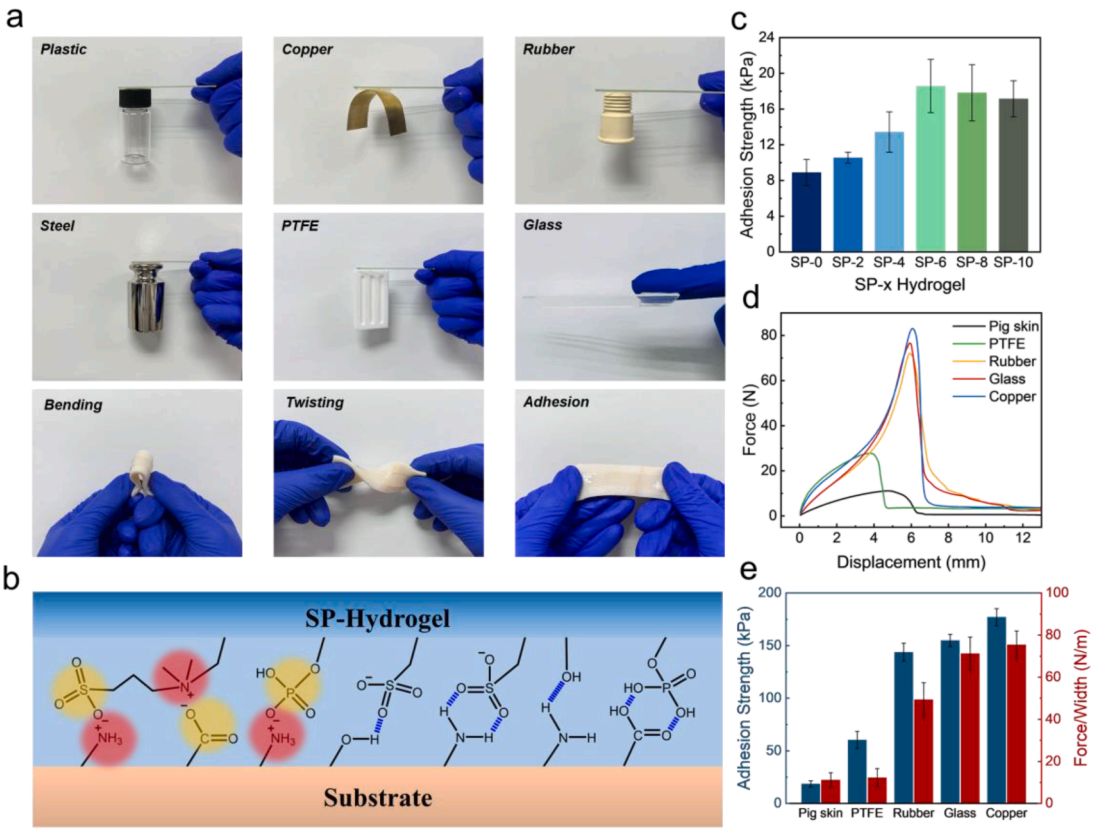

Fig. 3. Adhesive behaviors of SP-x hydrogels. (a) Photographs of SP-6 hydrogels adhering onto the surfaces of various organic and inorganic materials, including plastic, copper, rubber, steel, PTFE, and glass. SP-6 hydrogel adhering on pig skin can be bent and twisted while maintaining good integration. (b) Proposed mechanism of SP-x hydrogels adhering to substrate surfaces. (c) Adhesive strength of SP-x hydrogels onto pig skin. (d) Representative force-displacement curve, and (e) adhesive strength and peeling strength of SP-6 hydrogel onto pig skin, PTFE, rubber, glass, and copper, respectively.

were shown in Fig. 3d and 3e, respectively. As can be seen, high adhesive strength (>140.0 kPa) was achieved for SP-6 hydrogel on typical organic and inorganic substrates (i.e., 143.8 kPa, 154.9 kPa, and 177.0 kPa on rubber, glass, and copper, respectively). Surprisingly, the adhesive strength of SP-6 hydrogel on the surface of PTFE, a low surface energy synthetic material that is commonly difficult to attach to [30], reached up to 60.4 kPa. The results of the 90° peeling test also showed a high adhesion strength of the SP-6 hydrogel to be peeled off from the various substrates, and the peeling strengths were 11.1 N/m, 12.3 N/m, 49.3 N/m, 71.3 N/m, and 75.4 N/m on pig skin, PTFE, rubber, glass, and copper, respectively (Fig. 3e). Meanwhile, there was no significant reduction in the adhesion strength of SP-6 hydrogel on the various materials was observed after 5 cycles (Fig. S3). The reusability can be attributed to the synergistic effect of multiple non-covalent interactions between the SBMA groups and PA molecules of the hydrogel and the functional groups on the substrate surface. The results above revealed that SP-x hydrogel had universal and robust adhesion properties to a variety of materials, and was promising for wearable sensor applications.

3.3. Ionic conductivity and mechanical responsiveness of SP-x hydrogel

The ionic conductivity of hydrogels is a determining characteristic for skin sensor applications. The conductivity of pure polySBMA hydrogel (SP-0) was 0.04 S/m, which is too low to be used for electrical sensing applications. The addition of PA significantly improved the conductivity of the hydrogel (Fig. 4a). The conductivity increased from 1.69 S/m of SP-2 hydrogel to a maximum of 2.44 S/m of SP-6, which was 60 times that of SP-0. The EIS measurement also showed a much lower electrical resistance of SP-6 compared to SP-0 (Fig. S4). This is envisioned due to the large amount of free H^+ ions generated from the ionized PA in the hydrogel. The H^+ ions could form a directional migration through the polySBMA matrix under an electric field, which gives an intrinsic conductive characteristic to the SP-x hydrogels. However, when the content of PA further increased, the conductivity of the hydrogel reduced slightly to 1.46 S/m of SP-10. This is probably because of a synergistic effect of the restriction of PA ionization and a high cross-linking density due to the high concentration of PA in the hydrogel [17,20].

Because of its excellent mechanical properties, adhesion properties, and ionic conductivity, the potential of SP-6 hydrogel as a flexible sensor was further studied. First, the change in the resistance of SP-6 hydrogel after uniaxial stretching at a constant voltage of 0.5 V was measured (Fig. 4b). The relative resistance change ($\Delta R/R_0$) increased with increasing tensile strain, which fitted well with the quadratic equation (Fig. 4b). It is speculated that the network of the SP-6 hydrogel was relatively loose in its original state, allowing the ions to move freely and resulting in high conductivity. When the hydrogel was stretched, the conductive channel of ion transport was elongated and narrowed (Fig. S5a) [31,32], limiting the transportation of free ions and resulting in an increase in the resistance of the hydrogel. Correspondingly, the resistance of the hydrogel increased. Correspondingly, the strain sensitivity, also known as the gauge factor (GF), increased significantly from 1.91 at 0.2% strain to 9.72 at 400% strain, suggesting that the hydrogel was highly sensitive.

The compression sensing performance of SP-6 hydrogel is shown in Fig. 4c. When the compression strain was increased from 0 to 6.8% (corresponding compressive stress of ~19.5 kPa), the sensitivity increased dramatically from 1.08 to 10.62, demonstrating its excellent sensitivity. When the hydrogel was compressed, the length of the ion

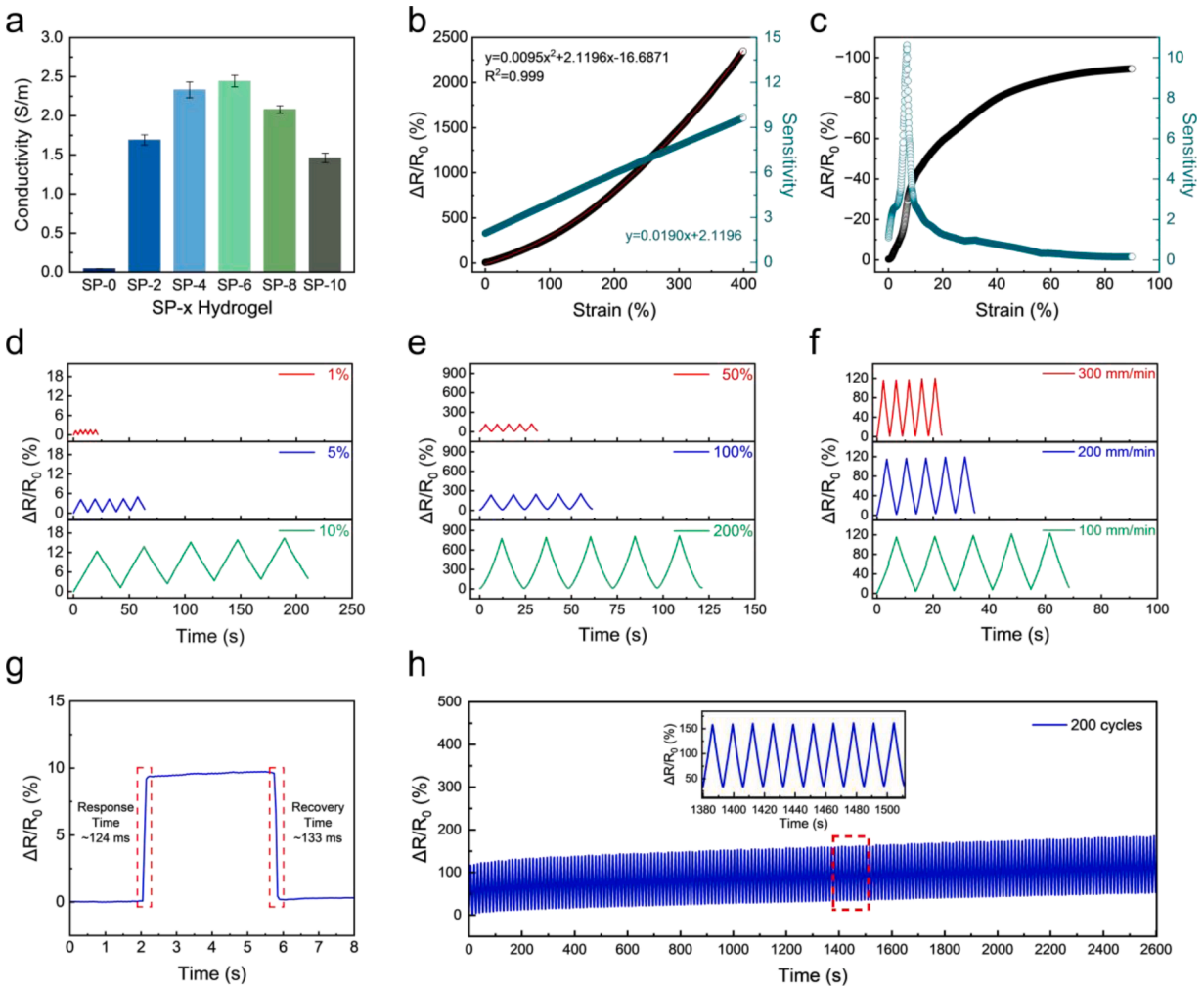

Fig. 4. (a) Ionic conductivity of SP-x hydrogels. Dependence of the relative resistance change ratio and sensitivity of the hydrogel on (b) tensile strain and (c) compressive strain. Relative resistance changes of SP-6 hydrogel under various tensile strains, including (d) small strains from 1% to 10%, and (e) large strains from 50% to 200%. (f) Relative resistance changes of SP-6 hydrogel stretched repeatedly to a strain of 50% at different strain speeds. (g) Response and recovery time of the relative resistance changes of SP-6 hydrogel stretched at a strain of 8%. (h) Cycling electric stability measurement of SP-6 hydrogel stretched at a strain of 50% for 200 cycles.

path became shorter, and the cross-sectional area increased (Fig. S5a), resulting in a decrease in resistance. The remarkable sensitivity at a low compressive strain range implied that the hydrogel may be used to detect subtle body motions. For example, when adhered to the finger, the flexible sensor integrated with SP-x hydrogels has the potential to receive human-like tactile feedback, such as recognizing finger taps on a keyboard, and determining the stiffness of various surfaces by pressing on them.

Notably, the hydrogel exhibited high sensitivity in a wide range of strains from 1% to 200% (Fig. 4d and 4e) and the relative resistance signals remained stable when the hydrogel was stretched repeatedly at various strain speeds (Fig. 4f). Based on the intensity of the peak response signal and the interval between adjacent waveforms, the amplitude and frequency of strains can be identified and detected. To further investigate the electrical properties of the hydrogels, a demonstration was built by connecting a light-emitting diode (LED) to a direct current power supply using SP-6 hydrogels (Fig. S5b). The brightness of LED changes in response to the mechanical deformation of the hydrogel in a cyclic process (Fig. S6), demonstrating the excellent strain-sensing capability of hydrogels. When the hydrogel was stretched, the relative resistance increased within 124 ms, and recovered within 133 ms, demonstrating the fast responsiveness and recovery capability of the hydrogel (Fig. 4g). This responsiveness was faster and the recovery time was shorter than the polyacrylamide/phytate-chitosan hydrogels (~290 ms) and cellulose nanocrystal/phytic acid hydrogels (342~365 ms) reported previously [17,18]. More notably, when the hydrogel was stretched by 50% strain repeatedly for 200 cycles over 2600 s, the relative resistance value exhibited good repeatability and low fluctuation (Fig. 4h), revealing the high electrical stability of the hydrogel. This is because in the deformation process, the dynamic noncovalent bonds in networks are readily fractured and serve as reversible "sacrificial bonds" to participate in energy dissipation via dissociation and/or reconstruction (Fig. S2d), resulting in high toughness and excellent self-recovery behavior of the SP-x hydrogels.

3.4. Sensor for the detection of body motions and biofluids

In view of the excellent mechanical properties, robust tissue adhesion, high transparency, stable conductivity, and outstanding sensitivity of the SP-6 hydrogel, its potential application as a wearable epidermal sensor was investigated. Firstly, a piece of SP-6 hydrogel was attached to the finger joint to detect the bending motion (Fig. 5a). The relative resistance of the hydrogel sensor increased as the bending angle of the finger increased from 0° to 90°, which was caused by the elongation of the hydrogel, and vice versa. The relative resistance changes of the hydrogel sensor could also be expressed continuously and steadily with

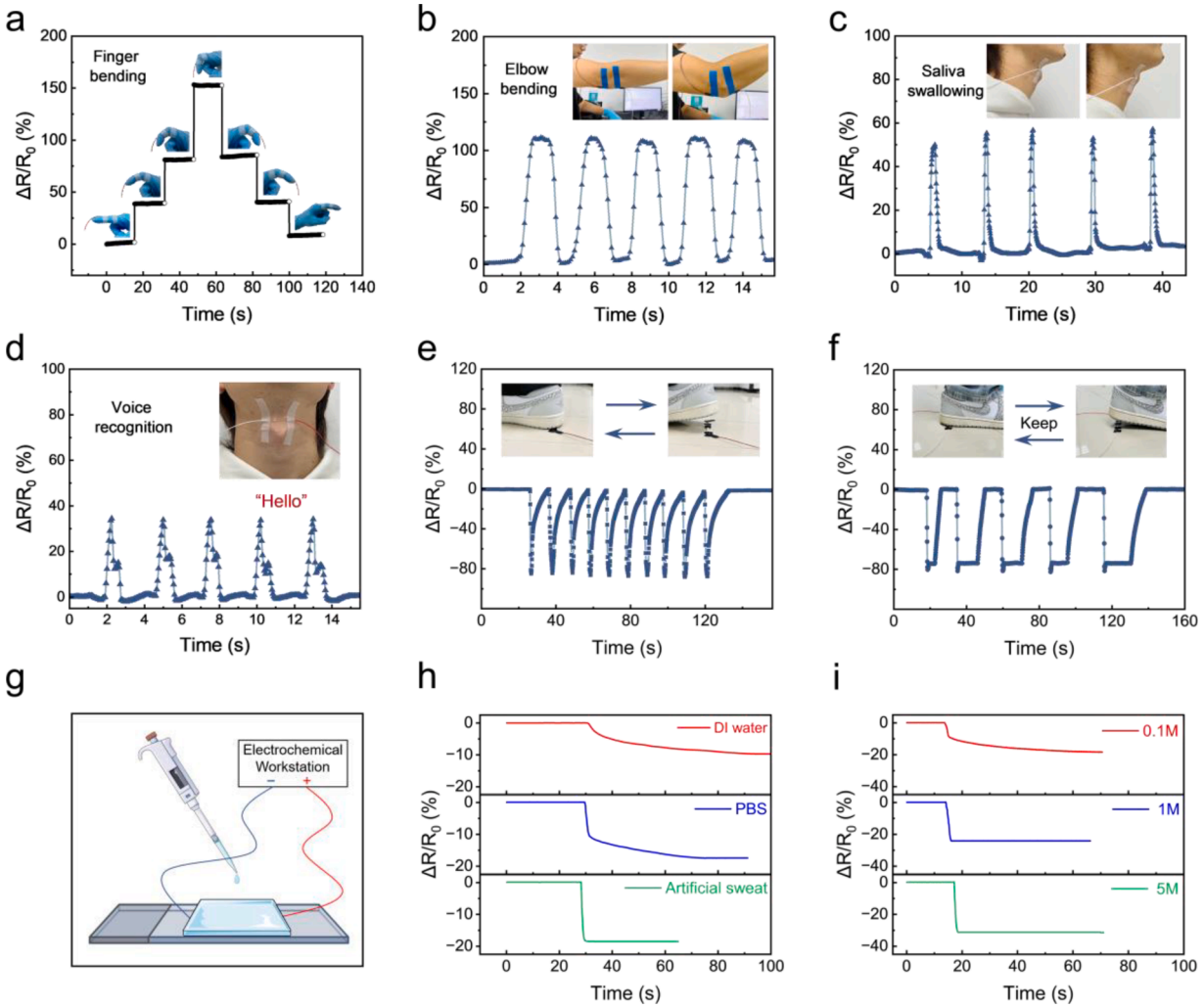

Fig. 5. Sensing performance of SP-6 hydrogel-based multifunctional flexible sensor. Relative resistance changes of sensors versus time for real-time monitoring of various human motions: (a) bending and releasing the forefinger at varying angles, and (b) flexion and extension of the elbow. Sensing the subtle muscle movements of the throat as the volunteer (c) swallowed saliva, and (d) said the words "Hello". Sensing foot weight applied (e) intermittently and (f) continuously to the sensors. (g) Schematic illustration of the setup with hydrogel for monitoring physiological fluids. Relative resistance changes of hydrogel after droplets of (h) various types of solutions, and (i) NaCl solutions with different concentrations (0.1, 1, and 5 mol/L) were applied.

various bending states of the elbow (Fig. 5b), and a brief peak of changes was observed during quick motions like swallowing saliva (Fig. 5c). In addition, the corresponding electrical signal showed a regular double-peaked shape with the articulation of the dissyllabic word "hello" (Fig. 5d). Furthermore, the potential of the hydrogel sensor to detect compression motion was investigated by placing the hydrogel beneath the feet and lifting at different intervals (Fig. 5e and 5f). When the hydrogel sensor was stepped on, the relative resistance significantly decreased because of the formation of a short conductive path inside the hydrogel. However, when the compression was removed, it took a relatively longer time to restore to its original value, which could be attributed to the energy dissipation during the compression process. Anyway, these findings demonstrated the remarkable capability of the hydrogel sensor to discriminate the variation of body motions, as it can detect both large-scale movements (elbow bending and compression motions) and small-scale movements (fingers bending, saliva swallowing, and speaking).

Tracking the changes in physiological fluid from the body during exercise can obtain real-time information related to human health and activity, reducing the risk of soft tissue injury, dehydration, or spasms [33,34]. In order to explore the applicability of hydrogel as a fluid sensor to detect the skin microenvironment, a droplet (~10 μL) of deionized water, PBS, artificial sweat, and NaCl solution were dropped onto a piece of SP-6 hydrogel, and the relative resistance of the hydrogel was recorded (Fig. 5g). As can be seen from Fig. 5h, the relative resistance of the hydrogel sensor decreased and gradually reached equilibrium after the fluids dropped onto the SP-6 hydrogel surface. However, the relative resistance showed different decreasing trends due to the different migration capabilities of the ions in the different liquids. Interestingly, when deionized water was added, the relative resistance of the hydrogel sensor also decreased visibly, most likely due to that the water molecules penetrated the hydrogel and created more migration paths for the conducting ions, which in turn improved the conductivity of the hydrogel. In addition, it was noted that the hydrogel sensor not only detected different types of fluids, but also distinguished the concentration of solutes in the solution. As shown in Fig. 5i, the relative resistance of the hydrogel sensor decreased more rapidly when the concentration of NaCl solution increased from 0.1 M to 5 M. This could be attributed to the penetration of Na^+ and Cl^- ions into the hydrogel, which increased the concentration of conductive ions and enhanced the conductivity of the hydrogel. The results have demonstrated that the SP-6 hydrogel could potentially be employed as a sensor for monitoring physiological fluids.

3.5. Anti-freezing properties and long-term stability of SP-x hydrogel

In a sub-zero environment, water in the hydrogel forms ice crystals, which extrude macromolecular chains, damage the structure, and impair the performance of the hydrogel, resulting in the loss of mechanical properties, light transmittance, and conductivity of sensors. Hence, maintaining the elasticity and adaptability of hydrogel at sub-zero temperatures is critical for its practical application. SP-6 hydrogel was stored at different temperatures (-80 °C to 20 °C) for 24 h and the morphology of the hydrogel was shown in Fig. 6a. The SP-6 hydrogel remained soft at 20 °C, 0 °C, and -40 °C. Despite a slight loss in transparency after stored at -40 °C, the hydrogel could still be twisted to demonstrate good flexibility. The SP-6 hydrogel had completely turned white after stored at -80 °C, and cracking could be observed upon twisting. The tensile and compressive properties of SP-6, and SP-8, and SP-10 hydrogels at -20 °C (Fig. S7a and S7b) were comparable to those at room temperature (Fig. 2b and 2c). The adhesive strength of SP-6 hydrogel on glass showed some decline at -20 °C (Fig. S7c), possibly due to the frozen of a small amount of internal water, but it still maintained an excellent adhesive strength of 132.0 kPa. The GF value of SP-6 hydrogel slightly decreased to 8.63 at -20 °C (Fig. S7d), which is probably because the molecular chains of the hydrogel moved slowly at sub-zero temperatures, thus reducing its sensitivity. The freezing tolerance of SP-x hydrogels was measured using DSC (Fig. 6b). As can be seen, the SP-0 hydrogel could withstand temperatures below -20 °C, which was because the super-hydrophilic zwitterionic polySBMA chains could firmly bind water molecules through long-range electrostatic interactions, thus inhibiting icing during freezing [8]. With the addition of PA, the hydrogel showed enhanced anti-freezing performance. SP-6 hydrogel showed an exothermic peak at -59.6 °C, which was far lower than that of SP-0 hydrogel, indicating the ice suppression effect of PA in the hydrogel. The exothermic peak of the SP-8 and SP-10 hydrogels even disappeared in the temperature range of 40 °C to -89 °C. The above results showed that the formation of ice crystals in the SP-x hydrogel was greatly suppressed, mostly likely due to the integration of PA into the water as the cosolvent promoted the water retention of hydrogels, ascribed to the formation of strong hydrogel bonding interactions between PA and water molecules, thereby giving the SP-x hydrogel remarkable anti-freezing capability (Fig. 6c).

To investigate the potential applicability of the hydrogel as a sensor in a cold environment, the ionic conductivity of the SP-6 hydrogel at temperatures varying from 20 °C to -80 °C was evaluated. The conductivity of SP-6 hydrogel decreased from 2.44 S/m at 20 °C to 1.45 S/m at 0 °C, and further to 0.32 S/m at -20 °C (Fig. 6d). The decrease in the conductivity of hydrogel with lowering temperature could be attributed to that the low temperature and the formed ice crystals would impede or hinder ion migration in the hydrogel [35–37]. Nevertheless, even at -40 °C, the conductivity of the SP-6 hydrogel maintained at 0.20 S/m, which was comparable to the previous works [38–40], indicating that the SP-6 hydrogel holds tremendous promise for future applications under extreme low temperature conditions.

To investigate the performance of SP-x hydrogel after long-term storage, it was incubated at room temperature with a relative humidity of 60% for 7 days. The tensile properties of the hydrogels (Fig. S7e) did not change significantly compared to that of the as-prepared samples (Fig. 2b). The adhesive strength of SP-6 hydrogel on glass (Fig. S7f and S7g) also showed no obvious change compared to that of the as-prepared SP-x hydrogels (Fig. 3e). The GF value of SP-6 hydrogel after long-term storage showed satisfying sensitivity (GF=9.22) (Fig. S7h), indicating the long-term stability of the hydrogels.

Under all the conditions, the SP-6 hydrogel possesses fast stress-strain responsiveness. The response time and recovery time of SP-6 were 166 and 254 ms at -20 °C, 190 and 297 ms after storage for 7 days (Fig. 6e). The SP-6 hydrogels after being stored at room temperature for 7 days or -20 °C for 24 h could still be utilized as flexible wearable sensors to record the finger bending (Fig. 6f). It can be found that the finger bending signals recorded by SP-6 hydrogel sensor were basically consistent with that of the as-prepared hydrogel (Fig. 5a). The results showed that the addition of PA could successfully endow the hydrogel with excellent anti-freezing properties and long-term stability. The SP-6 hydrogel still possesses good mechanical, adhesion, conductivity, sensitivity, and strain sensing functions at low temperature or long-term placement conditions, indicating that it has great potential for application in extreme environments or after long-term storage.

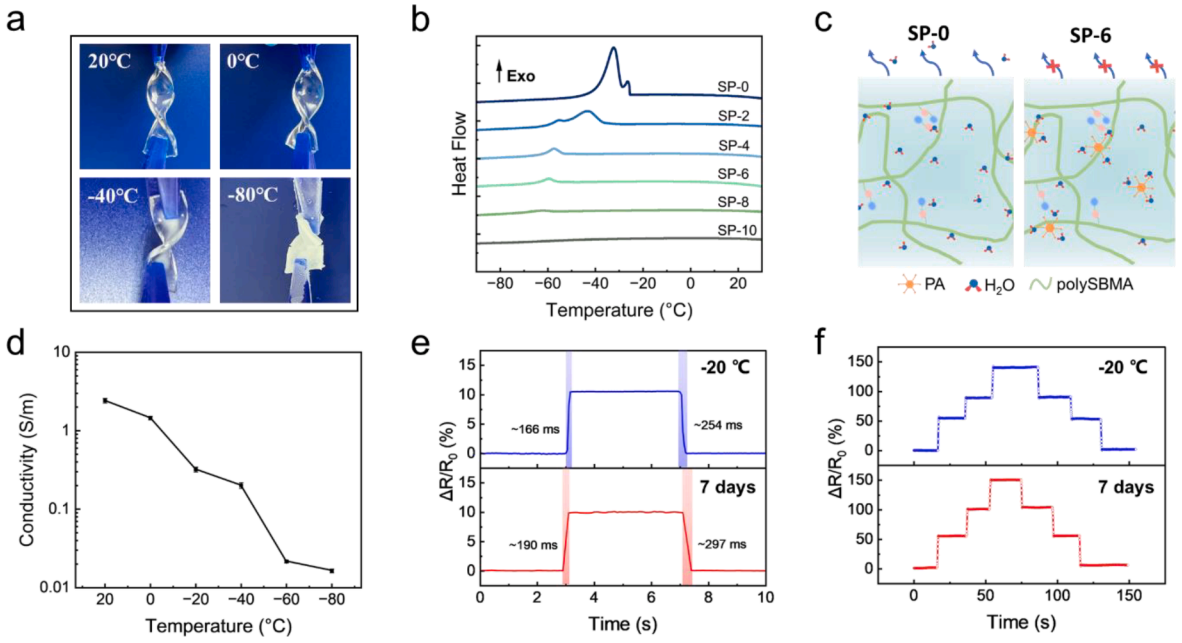

Fig. 6. (a) Photographs of SP-6 hydrogels after storing at 20 °C, 0 °C, -40 °C, and -80 °C for 24 h and then twisted. (b) DSC curves of SP-x hydrogels. (c) Schematic illustration of water retention property of SP-6 hydrogel. (d) Conductivity of the SP-6 hydrogel measured at different temperatures (20 °C to -80 °C). (e) Response and recovery time of the relative resistance changes of SP-6 hydrogel stretched at -20 °C or after storage for 7 days. (f) Relative resistance changes of SP-6 hydrogel as bending and releasing the forefinger after being placed at -20 °C or after storage for 7 days.

3.6. Antibacterial and biocompatibility of SP-x hydrogel

A wearable electronic device is required to attach directly to the skin for precious collection and transmission of electrical signals. However, direct and prolonged skin contact with the device may raise the risk of bacterial infections and allergic reactions, severely limiting the applicability of wearable sensors. As a result, antibacterial properties and biocompatibility are essential to extending the service life of the device [41]. Fig. 7a and 7b visually showed the antibacterial effect of SP-x hydrogels against *E. coli.* and *S. aureus* in the zone of inhibition tests. No inhibition zone was observed around the SP-0 hydrogel, while obvious [7] inhibition zones were observed around the SP-6 hydrogel (Fig. 7a), indicating that the addition of PA could endow hydrogels with significant antibacterial function. The remarkable antibacterial properties of the hydrogel were mainly attributed to PA molecules, which can act on the bacterial cell walls through its powerful ability to chelate metals and proteins, leading to inhibition of cell wall synthesis, cell membrane damage, and subsequent bacterial death [23–25]. In addition, the hydrogen ions (H^+) released by PA could also penetrate bacterial cells and rupture the organelles [17]. Based on the excellent antibacterial property of PA, the antibacterial zone of the hydrogel increased with the increase in PA content (Fig. 7b). The results confirmed that the SP-x hydrogels had a strong inhibitory effect on both Gram-positive bacteria and Gram-negative bacteria. The cytocompatibility of the hydrogels was assessed using the extract method. It was found that the extract of the SP-10 hydrogel showed slight cytotoxicity (76% of cell viability), while the extracts of other hydrogels (i.e., SP-0, SP-2, SP-4, and SP-6) showed good cytocompatibility (Fig. 7c).

Skin irritation test was also conducted to evaluate the biocompatibility of the hydrogels (Figs. 7d, 7e and S8). No erythema, eschar, edema, or inflammatory infiltration was observed on the skins in the SP-0 hydrogel group. Slight erythema on the mouse skin in the SP-6 hydrogel group after 48 h was observed. H&E staining images showed a small amount of inflammatory cells in the SP-6 hydrogel groups at 72 h (Figs. 7e and S8), whereas the epidermis was intact. Thanks to the good antibacterial properties and cell biocompatibility, as well as the mild

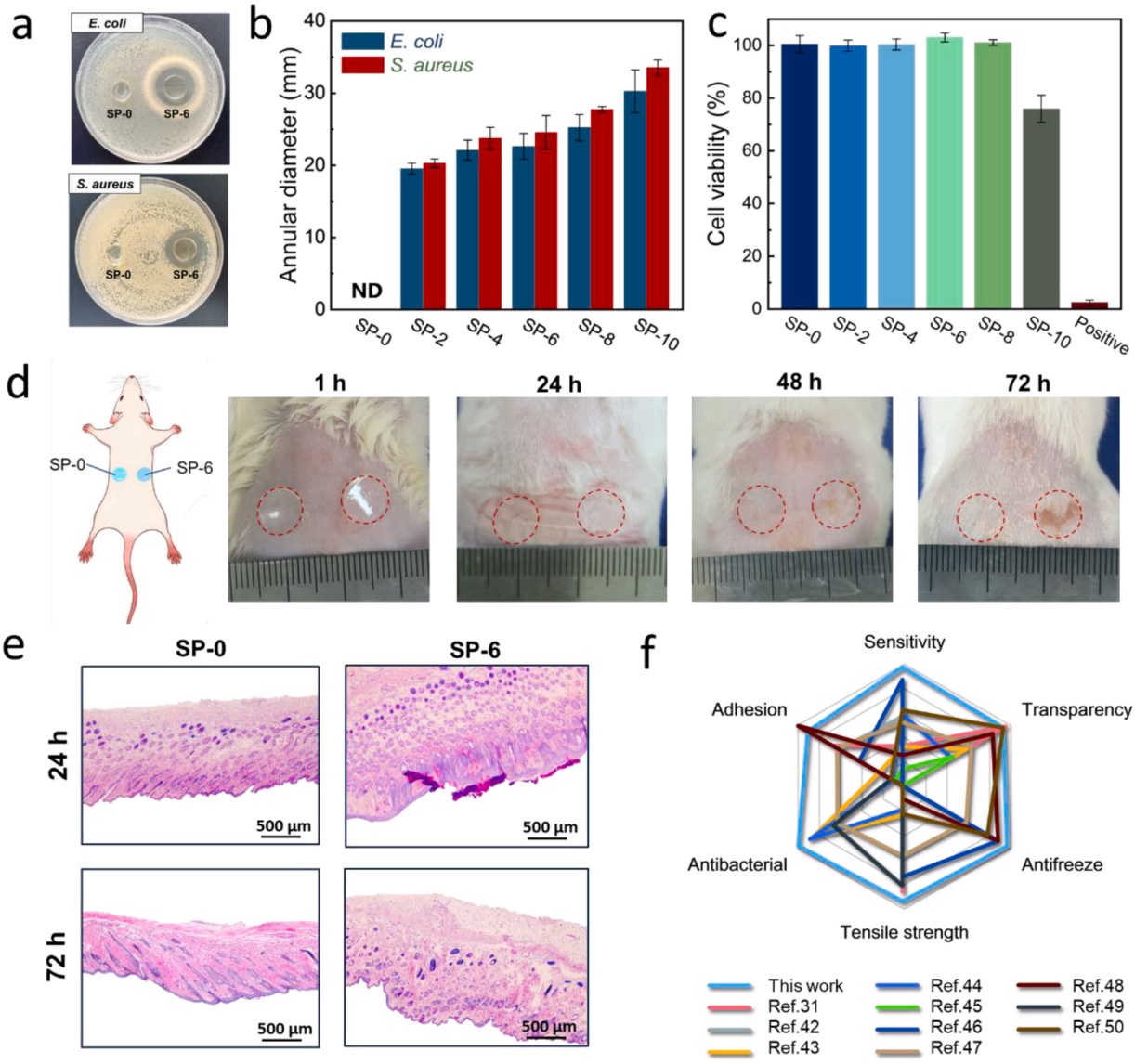

Fig. 7. (a) Digital photos of zone of inhibition test of SP-6 hydrogel against *E. coli* and *S. aureus*. (b) The diameters of the inhibition zone around different SP-x hydrogels. (c) Viability of NIH/3T3 fibroblasts after incubating in extracts of SP-x hydrogels for 24 h. (d) Schematic illustration of the skin irritant experiment, and digital photos of the mouse skin after treated with SP-0 and SP-6 hydrogels for different time. (e) H&E staining images of tissue on the treated site. (f) Radar chart of the comprehensive performance of the reported various hydrogel-based flexible sensors in terms of sensitivity, transparency, anti-freezing, tensile strength, antibacterial, and adhesion performances.

irritant response of the SP-x hydrogels, they have significant potential as a wearable sensor that can directly contact the skin, and can be further developed for various applications.

It is worth mentioning that it is difficult to achieve a simultaneous combination of ideal mechanical properties, high transparency, tissue adhesiveness, conductivity, antibacterial properties, and good biocompatibility in the various previously reported hydrogels [31,42–50], whereas the SP-x hydrogel developed in this study showed advantages in integrating the above-mentioned properties (Fig. 7f). Thus, the SP-x hydrogels show a significant advancement in the optimization of multifunctional ionic sensors.

4. Conclusions

In this study, we developed a novel ionic conductive PA-reinforced polySBMA hydrogels with self-adhesive, ionically conductive, environmentally tolerant and antibacterial abilities by introducing the conductive PA. The formation of abundant hydrogen bonds and electrostatic interactions between PA and SBMA improved the mechanical properties. Due to the ionization of PA, hydrogels exhibited extraordinary electrical conductivity (2.44 S/m). The incorporated PA could strongly bind water molecules and chelate metal ions or proteins, endowing the hydrogel with outstanding anti-freezing properties, long-term stability and antibacterial ability. Besides, the SP-x ionic conductive hydrogels exhibited excellent adhesion and could be applied as a wearable sensor which was demonstrated to monitor human body motions and voice recognition in real time. Therefore, the SP-x hydrogel exhibited a huge potential in the field of next-generation wearable intelligent sensors and human-machine interactions.

CRediT authorship contribution statement

Zhenlin Zuo: Writing – original draft, Validation, Resources, Methodology, Investigation, Formal analysis, Data curation, Conceptualization. **Lei Song:** Validation, Investigation, Formal analysis, Data curation. **Longxing Niu:** Writing – review & editing, Validation, Investigation, Formal analysis. **Rong Wang:** Writing – review & editing, Supervision, Project administration, Funding acquisition, Formal analysis, Conceptualization.

Declaration of competing interest

The authors declare that they have no known competing financial interests or personal relationships that could have appeared to influence the work reported in this paper.

Data availability

Data will be made available on request.

Acknowledgments

This work was supported by the Youth Innovation Promotion Association CAS (2021296), Key Research and Development Program of Ningbo (2022Z132), and Foundation of Director of Ningbo Institute of Materials Technology and Engineering CAS (2021SZKY0301).

Supplementary materials

Supplementary material associated with this article can be found, in the online version, at doi:10.1016/j.apmt.2024.102147.

References

[1] Y. Jiang, A.A. Trotsyuk, S. Niu, D. Henn, K. Chen, C.C. Shih, M.R. Larson, A. M. Mermin-Bunnell, S. Mittal, J.C. Lai, A. Saberi, E. Beard, S. Jing, D. Zhong, S. R. Steele, K. Sun, T. Jain, E. Zhao, C.R. Neimeth, W.G. Viana, J. Tang, D. Sivaraj, J. Padmanabhan, M. Rodrigues, D.P. Perrault, A. Chattopadhyay, Z.N. Maan, M. C. Leeolou, C.A. Bonham, S.H. Kwon, H.C. Kussie, K.S. Fischer, G. Gurusankar, K. Liang, K. Zhang, R. Nag, M.P. Snyder, M. Januszyk, G.C. Gurtner, Z. Bao, Wireless, closed-loop, smart bandage with integrated sensors and stimulators for advanced wound care and accelerated healing, Nat. Biotechnol 41 (2023) 652–662.

[2] B. Song, X. Dai, X. Fan, H. Gu, Wearable Multifunctional organohydrogel-based electronic skin for sign language recognition under complex environments, J. Mater. Sci. Technol. 181 (2024) 91–103.

[3] L. Zhao, Q. Ling, X. Fan, H. Gu, Self-healable, adhesive, anti-drying, freezing-tolerant, and transparent conductive organohydrogel as flexible strain sensor, triboelectric nanogenerator, and skin bArrier, ACS Appl. Mater. Interfaces 15 (2023) 40975–40990.

[4] B. Song, X. Fan, J. Shen, H. Gu, Ultra-stable and self-healing coordinated collagen-based multifunctional double-network organohydrogel e-skin for multimodal sensing monitoring of strain-resistance, bioelectrode, and self-powered triboelectric nanogenerator, Chem. Eng. J. 474 (2023) 145780.

[5] T. Zhu, Y. Ni, G.M. Biesold, Y. Cheng, M. Ge, H. Li, J. Huang, Z. Lin, Y. Lai, Recent advances in conductive hydrogels: classifications, properties, and applications, Chem. Soc. Rev 52 (2023) 473–509.

[6] B. Song, Z. Ren, H. Gu, Totally dynamically cross-linked dual-network conductive hydrogel with superb and rapid self-healing ability for motion detection sensors, Mater. Today Commun. 35 (2023) 105919.

[7] J. Liu, X. Fan, D. Astruc, H. Gu, Robust conductive skin hydrogel e-skin constructed by top–down strategy for motion-monitoring, Collagen & Leather 5 (2023) 17.

[8] Q. Li, C. Wen, J. Yang, X. Zhou, Y. Zhu, J. Zheng, G. Cheng, J. Bai, T. Xu, J. Ji, S. Jiang, L. Zhang, P. Zhang, Zwitterionic biomaterials, Chem. Rev 122 (2022) 17073–17154.

[9] M. Zhang, P. Yu, J. Xie, J. Li, Recent advances of zwitterionic-based topological polymers for biomedical applications, J. Mater. Chem. B 10 (2022) 2338–2356.

[10] X. Hu, P. Zhang, J. Liu, H. Guan, R. Xie, L. Cai, J. Guo, L. Wang, Y. Tian, X. Qiu, A self-association cross-linked conductive zwitterionic hydrogel as a myocardial patch for restoring cardiac function, Chem. Eng. J. 44 (2022) 136988.

[11] X. Pei, H. Zhang, Y. Zhou, L. Zhou, J. Fu, Stretchable, self-healing and tissue-adhesive zwitterionic hydrogels as strain sensors for wireless monitoring of organ motions, Mater. Horiz. 7 (2020) 1872–1882.

[12] Q. Fu, S. Hao, L. Meng, F. Xu, J. Yang, Engineering self-adhesive polyzwitterionic hydrogel electrolytes for flexible zinc-ion hybrid capacitors with superior low-temperature adaptability, ACS. Nano 7 (2020) 18469–18482.

[13] K. Fang, Q. Gu, M. Zeng, Z. Huang, H. Qiu, J. Miao, Y. Fang, Y. Zhao, Y. Xiao, T. Xu, R.P. Golodok, V.V. Savich, A.P. Ilyushchenko, F. Ai, D. Liu, R. Wang, Tannic acid-reinforced zwitterionic hydrogels with multi-functionalities for diabetic wound treatment, J. Mater. Chem. B 10 (2022) 4142–4152.

[14] J. Yang, Z. Xu, J. Wang, L. Gai, X. Ji, H. Jiang, L. Liu, Antifreezing zwitterionic hydrogel electrolyte with high conductivity of 12.6 mS cm^{-1} at -40°C through hydrated lithium ion hopping migration, Adv. Funct. Mater. 31 (2021) 2009438.

[15] R. Wang, S. Guo, Phytic acid and its interactions: contributions to protein functionality, food processing, and safety, Compr. Rev. Food Sci. Food Saf. 20 (2021) 2081–2105.

[16] J. Emsley, S. Niazi, The structure of myo-inositol hexaphosphate in solution: ^{31}P N. M.R. investigation, Phosphorus. Sulfur. Silicon. Relat. Elem. 10 (1981) 401–407.

[17] Q. Zhang, X. Liu, J. Zhang, L. Duan, G. Gao, A highly conductive hydrogel driven by phytic acid towards a wearable sensor with freezing and dehydration resistance, J. Mater. Chem. A 9 (2021) 22615–22625.

[18] Z. Wang, Z. Ma, S. Wang, M. Pi, X. Wang, M. Li, H. Lu, W. Cui, R. Ran, Cellulose nanocrystal/phytic acid reinforced conductive hydrogels for antifreezing and antibacterial wearable sensors, Carbohydr. Polym. 298 (2022) 120128.

[19] S. Zhang, Y. Zhang, B. Li, P. Zhang, L. Kan, G. Wang, H. Wei, X. Zhang, N. Ma, One-step preparation of a highly stretchable, conductive, and transparent poly(vinyl alcohol)-phytic acid hydrogel for casual writing circuits, ACS Appl. Mater. Interfaces 11 (2019) 32441–32448.

[20] C. Liu, R. Zhang, Y. Wang, J. Qu, J. Huang, M. Mo, N. Qing, L. Tang, Tough, anti-drying and thermoplastic hydrogels consisting of biofriendly resources for a wide linear range and fast response strain sensor, J. Mater. Chem. A 11 (2023) 2002–2013.

[21] C. Lu, J. Qiu, M. Sun, Q. Liu, E. Sakai, G. Zhang, Simple preparation of carboxymethyl cellulose-based ionic conductive hydrogels for highly sensitive, stable and durable sensors, Cellulose 28 (2021) 4253–4265.

[22] Y. Nie, D. Yue, W. Xiao, W. Wang, H. Chen, L. Bai, L. Yang, H. Yang, D. Wei, Anti-freezing and self-healing nanocomposite hydrogels based on poly(vinyl alcohol) for highly sensitive and durable flexible sensors, Chem. Eng. J. 436 (2022) 135243.

[23] N.H. Kim, M.S. Rhee, Synergistic bactericidal action of phytic acid and sodium chloride against *Escherichia coli* O157:H7 cells protected by a biofilm, Int. J. Food Microbiol. 227 (2016) 17–21.

[24] P.M. Davidson, T.M. Taylor, S.E. Schmidt, Chemical preservatives and natural antimicrobial compounds, Food Microbiol. 30 (2012) 765–801.

[25] N.H. Kim, M.S. Rhee, Phytic acid and sodium chloride show marked synergistic bactericidal effects against nonadapted and acid-adapted *Escherichia coli* O157:H7 strains, Appl. Environ. Microbiol. 82 (2016) 1040–1049.

[26] W. Liu, R. Xie, J. Zhu, J. Wu, J. Hui, X. Zheng, F. Huo, D. Fan, A temperature responsive adhesive hydrogel for fabrication of flexible electronic sensors, npj Flex. Electron 6 (2022) 68.

[27] Y. Yu, H. Yuk, G.A. Parada, Y. Wu, X. Liu, C.S. Nabzdyk, k. Youcef-toumi, J. Zang, X. Zhao, Multifunctional "hydrogel skins" on diverse polymers with arbitrary shapes, Adv. Mater. 31 (2019) 1807101.
[28] L. Wang, G. Gao, Y. Zhou, T. Xu, J. Chen, R. Wang, R. Zhang, J. Fu, Tough, adhesive, self-healable, and transparent ionically conductive zwitterionic nanocomposite hydrogels as skin strain sensors, ACS Appl. Mater. Interfaces 11 (2019) 3506–3515.
[29] C.Y. Zou, X.X. Lei, J.J. Hu, Y.L. Jiang, Q.J. Li, Y.T. Song, Q.Y. Zhang, J. Li-Ling, H. Q. Xie, Multi-crosslinking hydrogels with robust bio-adhesion and pro-coagulant activity for first-aid hemostasis and infected wound healing, Bioact. Mater. 16 (2022) 388–402.
[30] Q. Guo, Y. Huang, M. Xu, Q. Huang, J. Cheng, S. Yu, Y. Zhang, C. Xiao, PTFE porous membrane technology: a comprehensive review, J. Membr. Sci 664 (2022) 121115.
[31] H. Wei, Z. Wang, H. Zhang, Y. Huang, Z. Wang, Y. Zhou, B.B. Xu, S. Halila, J. Chen, Ultrastretchable, highly transparent, self-adhesive, and 3D-printable ionic hydrogels for multimode tactical sensing, Chem. Mater 33 (2021) 6731–6742.
[32] Y. Zhang, T. Li, L. Miao, P. Kaur, S. Men, Q. Wang, X. Gong, Y. Fang, C. Zhai, S. Zhang, L. Zhang, L. Ye, A highly sensitive and ultra-stretchable zwitterionic liquid hydrogel-based sensor as anti-freezing ionic skin, J. Mater. Chem. A 10 (2022) 3970–3988.
[33] M.C. Brothers, M. DeBrosse, C.C. Grigsby, R.R. Naik, S.M. Hussain, J. Heikenfeld, S. S. Kim, Achievements and challenges for real-time sensing of analytes in sweat within wearable platforms, Acc. Chem. Res. 52 (2019) 297–306.
[34] J. Yoon, H.Y. Cho, M. Shin, H.K. Choi, T. Lee, J.W. Choi, Flexible electrochemical biosensors for healthcare monitoring, J. Mater. Chem. B 8 (2020) 7303–7318.
[35] L. Shi, K. Jia, Y. Gao, H. Yang, Y. Ma, S. Lu, G. Gao, H. Bu, T. Lu, S. Ding, Highly stretchable and transparent ionic conductor with novel hydrophobicity and extreme-temperature tolerance, Research 2020 (2020) 2505619.
[36] B. Song, X. Fan, H. Gu, Chestnut-tannin-crosslinked, antibacterial, antifreezing, conductive organohydrogel as a strain sensor for motion monitoring, flexible keyboards, and velocity monitoring, ACS Appl. Mater. Interfaces 15 (2023) 2147–2162.
[37] X. Fan, L. Zhao, Q. Ling, J. Liu, H. Gu, Mussel-induced nano-silver antibacterial, self-healing, self-adhesive, anti-freezing, and moisturizing dual-network organohydrogel based on SA-PBA/PVA/CNTs as flexible wearable strain sensors, Polymer 256 (2022) 125270.
[38] X. Zhang, C. Cui, S. Chen, L. Meng, H. Zhao, F. Xu, J. Yang, Adhesive ionohydrogels based on ionic liquid/water binary solvents with freezing tolerance for flexible ionotronic devices, Chem. Mater. 34 (2022) 1065–1077.
[39] Z. Liu, J. Zhang, J. Liu, Y. Long, L. Fang, Q. Wang, T. Liu, Highly compressible and superior low temperature tolerant supercapacitors based on dual chemically crosslinked PVA hydrogel electrolytes, J. Mater. Chem. A 8 (2020) 6219–6228.
[40] X. Zhao, F. Chen, Y. Li, H. Lu, N. Zhang, M. Ma, Bioinspired ultra-stretchable and anti-freezing conductive hydrogel fibers with ordered and reversible polymer chain alignment, Nat. Commun. 9 (2018) 3579.
[41] X. Fan, T. Ke, H. Gu, Multifunctional, ultra-tough organohydrogel e-skin reinforced by hierarchical goatskin fibers skeleton for energy harvesting and self-powered monitoring, Adv. Funct. Mater. 33 (42) (2023) 2304015.
[42] B. Wang, L. Dai, L.A. Hunter, L. Zhang, G. Yang, J. Chen, X. Zhang, Z. He, Y. Ni, A multifunctional nanocellulose-based hydrogel for strain sensing and self-powering applications, Carbohydr. Polym. 268 (2021) 118210.
[43] M. Pan, M. Wu, T. Shui, L. Xiang, W. Yang, W. Wang, X. Liu, J. Wang, X.Z. Chen, H. Zeng, Highly stretchable, elastic, antimicrobial conductive hydrogels with environment-adaptive adhesive property for health monitoring, J. Colloid Interface Sci. 622 (2022) 612–624.
[44] Z. Han, S. Chen, L. Deng, Q. Liang, X. Qu, J. Li, B. Wang, H. Wang, Anti-fouling, adhesive polyzwitterionic hydrogel electrodes toughened using a tannic acid nanoflower, ACS Appl. Mater. Interfaces 14 (2022) 45954–45965.
[45] S. Wu, Z. Shao, H. Xie, T. Xiang, S. Zhou, Salt-mediated triple shape-memory ionic conductive polyampholyte hydrogel for wearable flexible electronics, J. Mater. Chem. A 9 (2021) 1048–1061.
[46] Y. Liang, K. Wang, J. Li, H. Wang, X.Q. Xie, Y. Cui, Y. Zhang, M. Wang, C.S. Liu, Low-molecular-weight supramolecular-polymer double-network eutectogels for self-adhesive and bidirectional sensors, Adv. Funct. Mater. 31 (2021) 2104963.
[47] J. Wang, T. Dai, H. Wu, M. Ye, G. Yuan, H. Jia, Tannic Acid-Fe^{3+} activated rapid polymerization of ionic conductive hydrogels with high mechanical properties, self-healing, and self-adhesion for flexible wearable sensors, Compos. Sci. Technol. 221 (2022) 109345.
[48] Z. He, W. Yuan, Adhesive, stretchable, and transparent organohydrogels for antifreezing, antidrying, and sensitive ionic skins, ACS Appl. Mater. Interfaces 13 (2021) 1474–1485.
[49] L. Fan, L. Hu, J. Xie, Z. He, Y. Zheng, D. Wei, D. Yao, F. Su, Biosafe, self-adhesive, recyclable, tough, and conductive hydrogels for multifunctional sensors, Biomater. Sci 9 (2021) 5884–5896.
[50] Y. Gao, S. Gu, F. Jia, Q. Wang, G. Gao, "All-in-one" hydrolyzed keratin protein-modified polyacrylamide composite hydrogel transducer, Chem. Eng. J 398 (2020) 125555.